



Considering semi-crystallinity in molecular simulations of mechanical polymer properties – using nanoindentation of polyethylene as an example

Susanne Fritz 

FILK Freiberg Institute gGmbH, Meißner Ring 1–5, 09599 Freiberg, Germany.

Abstract

Molecular dynamic (MD) simulations have been used to investigate the response of semi-crystalline polymers in nanoindentation tests, using polyethylene (PE) as an example. To that purpose, semi-crystalline simulation boxes of linear PE with various chain lengths up to C2000 were created by homogeneous nucleation during the non-isothermal cooling of melts. The final crystallinity depended on the chain length and the cooling rate used and could be estimated using various parameters like density, fraction of bonds in trans conformation, and energy terms. The simulation boxes were transferred into surface models and subjected to nanoindentation tests using non equilibrium MD. This allowed the deformation behaviour of the material to be analysed directly. Strong dependencies on the crystallinity of the PE were found, which underlines the importance of considering crystallinity when investigating the mechanical properties of semi-crystalline polymers by means of simulations.

Keywords: MD, simulation, polymer, polyethylene, semi-crystalline, mechanical properties, crystallization, nanoindentation

1. Introduction

Molecular dynamics (MD) simulations have been widely used to analyse the mechanical properties and stress strain behaviour of polyethylene (PE) in uniaxial tensile tests (e.g., Higushi, 2019; Higuchi & Kubo, 2017; Hossain et al., 2010; Kim et al., 2014; Le, 2020; Monasse et al., 2008; Moyassari et al., 2019a, 2019b). From these simulations, Young's modulus or yield stresses have been calculated. The origin of yield point, strain softening, and strain hardening has been related to chain reordering, and the fracture behaviour has been analysed for systems of different sizes and compositions. Semi-crystallinity, as well as viscoelasticity and temperatures below and above glass transition, were concerned in such studies. However, to date simulations of nanoindentation tests with PE have been rare, and none have concerned with the semi-crystallinity of the PE.

Experimental nanoindentation tests are a useful means of determining the mechanical properties of surfaces in high spatial resolution. They are especially important when surface properties differ significantly from bulk properties, as is the case of coatings (e.g., PE on paper or textiles). Compared to the tensile test, the acting forces are very small, affecting only marginal volumes of the sample. Therefore, nanoindentation tests are the ideal method for analysing coatings, layered materials, individual grains, property gradients, or multiphase and composite systems. However, while indentation at the macroscopic and microscopic level is well understood, at the nanoscopic level there are still many open questions. This is especially true for polymers because of their viscoelastic properties (Christöfl et al., 2021; VanLandingham et al., 2001). That is why understanding nanoindentation of polymers at the atomistic level is crucial for the reliable and correct

* Author's email: susanne.fritz@ilkfreiberg.de.

ORCID ID: 0000-0002-5006-8826

© 2021 Authors. This is an open access publication, which can be used, distributed and reproduced in any medium according to the Creative Commons CC-BY 4.0 License requiring that the original work has been properly cited.

determination and interpretation of measurement data. For this purpose, MD simulations can be useful, as has been proven in the case of metals (Ruestes et al., 2017; Voyiadjis & Yaghoobi, 2017). Gibson (2014) reviewed experimental and simulation research of nanoindentation of polymers and stated that there were numerous atomistic simulation studies concerning metals and ceramics, but that molecular dynamic or multiscale simulations with polymers were rare. The situation has not changed much since then.

For polymers, PE is often used as a model substance within experiments or simulations because of its chemical simplicity, high production level, and the availability of material models (Ramos et al., 2018). Furthermore, for PE as the most common plastic in the world (*Poly(ethene)...*, 2017), there is great interest in understanding and predicting material properties and behaviour during processing and use. But, as for a semi-crystalline material with a glass transition temperature far beneath the operating temperature macroscopic simulations to that purpose are not quite simple. Due to the viscoelasticity, the mechanical response of the material is time and velocity dependent. Adhesion forces may lead to material deformation due to the low hardness of the polymer. Furthermore, different branching of the polymer chains leads to varying crystallinity between 50% and 90%, which strongly affects all mechanical properties of the PE (e.g., Rozanski & Galeski, 2013; Xu et al., 2016). Despite intensive research, many questions remain open concerning the origin and modelling of the mechanical properties of PE. It is even more problematic in terms of surface properties, as they are important for every kind of contact phenomena such as friction, adhesion, liability, and wear.

Molecular dynamics (MD) simulations can help to improve understanding of the underlying processes at the surfaces on the atomistic scale. In this way, they help to interpret experimental data and allow to develop macroscopic material models to predict the materials behaviour during processing and use. Especially, the simulation of nanoindentation tests are suitable to understand deformation behaviour and contact formation at the surface. Yashiro et al. (2006) simulated nanoindentation with a spherical indenter using an amorphous as well as an idealized, folded-chain crystalline polymeric model and highlighted the role of entropy during deformation. Hu et al. (2011, 2013) analysed the origin of greater values of Young's modulus and hardness in filled compared to pure PE as well as the influence of indenter shape on the mechanical properties obtained. Peng and Zeng (2017) derived an empirical hardness model for PE from molecular dynamic simulations. Meguid et al. (2018) investigated the contact behaviour of multilayered graphene-reinforced PE composite systems. To date, semi-crystallinity, which decisively determines the mechanical properties, especially above the

glass transition temperature, has not been taken into account in MD simulation studies on nanoindentation.

PE forms crystalline lamellae, which are arranged in a dendritic superstructure of some micrometres in size. To consider the whole structure is beyond the possibilities of atomistic simulations. In order to analyse semi-crystalline PE by MD simulations (e.g., for tensile tests), it is common practice to focus on single structure motives. For example, various authors start from a PE single crystal and introduce an amorphous, interlamellar phase by breaking some bonds and melting the inner part of the crystal with the help of Monte Carlo techniques while fixing the outer parts of the simulations box (e.g., Kim et al., 2014; Kumar et al., 2017; Lee & Rutledge, 2011; Monasse et al., 2008; Yeh et al., 2015, 2017). In this way, a layered, periodic system is created that can be exposed to different loads for the simulation. This procedure is fast and allows to adjust the content of loops, ties, and tailed molecules. But the boxes are anisotropic, which means that directionality has to be considered. The amorphous layer thickness is relatively large, and many aspects of the influence of the structure are neglected by considering only a small part of the structure. This procedure is especially suited to analyse the behaviour of amorphous interlayers. Alternatively, semi-crystalline simulation boxes can be obtained by homogeneous nucleation from the melt, but this procedure is rarely used, probably because of the high computational cost. Considerable work has focused on the crystallization behaviour of PE as a model substance for semi-crystalline polymers. But even these studies often only examine single molecules (e.g., Abu-Shark & Hussein, 2002; Doran & Choi, 2001; Gao et al., 2016; Liao & Jin, 1999; Ramos & Martínez-Salazar, 2011; Ramos et al., 2018; Sanmartín et al., 2012). There are only a few papers on nucleation and crystallization from the melt (Anwar & Schilling, 2015; Lacevic et al., 2008; Sanmartín et al., 2014; Wang et al., 2021) and high undercooling, coarse-graining techniques (Hall et al., 2020), preoriented melts (Ko et al., 2004), external forces (Lavine et al., 2003) or heterogeneous nucleation (Verho et al., 2018) are used to accelerate nucleation.

Higuchi & Kubo (2017) and Higushi (2019) created a multilayer, semi-crystalline model by crystallization from the melt with external forces and used it for the analysis of stress-strain behaviour. Moyassari et al. (2019a, 2019b) reported coarse-grained simulations of tensile tests with semi-crystalline PE blends, obtained by homogeneous nucleation. But although challenging in terms of computational time, homogeneous nucleation has some distinct advantages. Due to the number and random orientation of the crystallites the simulation boxes are isotropic. This eliminates the need to consider directionality. Interaction between different phases can be addressed in a better way. Despite the small size of the crystallites and the

lack of dendritic superstructure, polycrystalline systems provide good agreement with the experiment, showing that it is not the spherulitic structure but the lamellae on a smaller length scale that determine the deformation behaviour (Jabbari-Faro et al., 2015). Therefore, the aim of this paper is to describe how semi-crystalline simulation boxes of PE can be specifically prepared and characterised to investigate the mechanical and surface properties of PE at the atomic level and how semi-crystallinity affects the materials response in nanoindentation tests.

2. Materials and methods

2.1. Simulation procedure

For this research, molecular dynamics simulations (MD) were carried out. During MD simulations, the material is described at the atomic scale by the positions and properties of the atoms building it up. Via potential functions and force field parameters, the interaction energies and forces between the atoms are calculated. By integration of Newton's equation of motion and solving it for an infinitesimally small time step the change of the atomic positions due to the acting forces can be obtained. The dynamic evolution of the system can be assessed by an alternating process of calculating forces and positions over many time steps. Because of the tendency to minimize energy, the system will eventually evolve to equilibrium. By applying additional external forces processes can be simulated (NEMD, non equilibrium MD). The material properties can be obtained from atomic positions, velocities, forces, distributions, and movements by means of statistical thermodynamics. The principles are well established and described in more de-

tail elsewhere (Allen & Tildesley, 1987; Frenkel & Smit, 2001; Hill, 1987). The method is being further developed and used in various material areas (Hollingsworth & Dror, 2018; Lazim et al., 2020; Zhang et al., 2016).

MD simulations were performed using the GROMACS software package (Abraham et al. 2015; Berendsen et al., 1995; Gromacs 2020), running on NVIDIA Quadro P2000 graphic cards. The leap-frog-algorithm (Hockney et al., 1974) was used together with a time step of 3 fs to integrate the equation of motion. Equilibration simulations were performed with a smaller time step of 1 fs. Three-dimensional periodic boundary conditions were applied to simulate condensed material. Nonbonded interactions were cut off at 1 nm with the Verlet algorithm for neighbour searching (Páll & Hess, 2013). The temperature was controlled with the velocity-rescaling thermostat (Bussi et al., 2007), and pressure control to 1 bar was done with an anisotropic Berendsen barostat (Berendsen et al., 1984).

2.2. Polyethylene chains

For this work, linear, unbranched polyethylene (PE) chains with different chain lengths between 40 and 2000 carbon atoms were used. Interaction energies were calculated with the GROMOS 53a6 force field (Daura et al., 1998; Oostenbrink et al., 2004; Schuler et al., 2001), a united atom force field for hydrocarbons and biomolecules. In this force field, CH_n -groups are treated as units, which saves computation time by reducing the number of particles and allowing a larger time step to be used. The applied potential functions and force field parameters can be found in Table 1.

Table 1. Interaction functions and parameters used, taken from GROMACS user manual (Lindahl et al., 2021a) and GROMACS source code (Lindahl et al., 2021b)

Interaction potential	Parameter
Total potential energy $V_{pot} = V_b + V_a + V_d + V_{L_j}$	$m(\text{CH}_3) = 15.035 \text{ g/mol}$ $m(\text{CH}_2) = 14.027 \text{ g/mol}$
Fourth power bond potential $V_b = \frac{1}{4} k_{ij}^b (r_{ij}^2 - b_{ij}^2)^2$	$b = 0.153 \text{ nm}$ $k^b = 7.15 \cdot 10^6 \text{ kJ}/(\text{mol} \cdot \text{nm}^4)$
Cosine based angle potential $V_a(\theta_{ijk}) = \frac{1}{2} k_{ijk}^\theta (\cos(\theta_{ijk}) - \cos(\theta_{ijk}^0))^2$	$\theta^0 = 111^\circ$ $k^\theta = 530 \text{ kJ/mol}$
Periodic dihedral potential $V_d(\phi_{ijkl}) = k_\phi (1 + \cos(n\phi - \phi_s))$	$\phi_s = 0^\circ, n = 3$ $k_\phi = 5.92 \text{ kJ/mol}$
Lennard Jones potential $V_{L_j}(r_{ij}) = \frac{c_{ij}^{(12)}}{r_{ij}^{12}} - \frac{c_{ij}^{(6)}}{r_{ij}^6}$	$C_{\text{CH}_2}^{(6)} = 0.0074684164 \text{ kJ}/(\text{mol} \cdot \text{nm}^6)$ $C_{\text{CH}_2}^{(12)} = 3.3965584 \cdot 10^{-5} \text{ kJ}/(\text{mol} \cdot \text{nm}^{12})$ $C_{\text{CH}_3}^{(6)} = 0.0096138025 \text{ kJ}/(\text{mol} \cdot \text{nm}^6)$ $C_{\text{CH}_3}^{(12)} = 2.6646244 \cdot 10^{-5} \text{ kJ}/(\text{mol} \cdot \text{nm}^{12})$

PE chains were generated in an idealized, totally stretched form. All kinds of simulation models were then created as described below. For comparison reasons also theoretical models of fully crystalline and fully amorphous PE were built.

2.3. Procedure for preparation of bulk simulation boxes

The simulation boxes were created in a multi-stage process. Starting from one ideal, totally stretched PE chain a fully crystalline, dense-packed system was generated. By melting the crystalline system and cooling the melt with different cooling rates amorphous and semi-crystalline simulation boxes were obtained. The procedure is drawn schematically in Figure 1 and explained in detail below.

To generate crystalline simulation boxes, a certain number of identical PE chains in all-trans configuration were densely packed in parallel with the `gmgenbox` tool of the GROMACS package. The size of the simulation box was precalculated to achieve a volume corresponding to a mass density of 1000 kg/m^3 . Chains were regularly packed perpendicular to chain direction but with random variation of position in chain

direction to avoid predetermined breaking points. The simulation boxes were minimized and then equilibrated in the isothermal-isobaric ensemble (NpT) for 3 ns to obtain purely hypothetical models of a fully crystalline PE. On the one hand, these models were used as starting point for the preparation of all other models. On the other hand, they also served as comparative states for the evaluation of the calculated properties. The different systems are listed in Table 2.

In the next step, the crystalline models were melted with the help of simulated annealing. In this procedure, the reference temperature of the thermostat was continuously changed during the simulation, while an anisotropic barostat was used for pressure coupling. The crystalline model was heated above the melting point to provide the chains with energy and allow them to move, mix, entangle and take their coiled form. Different temperature profiles were tested to achieve satisfying results while saving simulation time. It was found that heating can be done in a very fast way without disadvantages (e.g., 300 ps). Since the chains were not allowed to break during the simulation, temperatures far above the melting temperature (e.g., 1000 K) could be used to accelerate mixing. For even higher temperatures, the time step had to be reduced to avoid crashes of the simulation and no further benefits were gained.

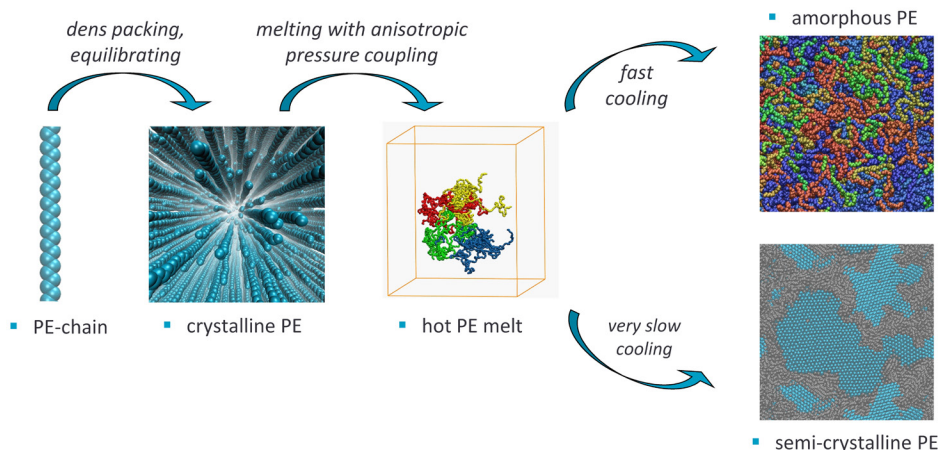


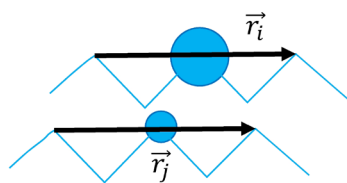
Fig. 1. Schematic overview of the model preparation procedure; only parts of the simulation boxes are shown for clarity

Table 2. Considered PE systems

Designation	Chain length [Carbon atoms]	Molecular weight [g/mol]	Number of chains
C40	40	567.58	7200
C80	80	1133.15	3600
C160	160	2264.29	1800
C200	200	2829.86	1500
C400	400	5657.70	1000
C2000	2000	28280.45	225

The longer the chains, the more time was needed to get a proper mixed system without preferred orientation. To control the melting state, changes in the radius of gyration, R_g , were monitored. Starting from the crystalline state the initial R_g was very large perpendicular to the chain direction and extremely small in the chain direction, which is altered during melting. In the final state of isotropic melt without preferred orientation the average components of R_g were equal in all three dimensions. This is shown in Figure 1 for the example of a fast equilibrating C40 system, where the proper melted state was already reached after 100 ps at 1000 K. The C160 system was only equilibrated after 2 ns and the C2000 system even needed 40 ns to reach a sufficient melting state. Thus, this method is not the fastest one to prepare an amorphous state. That is why, usually another and faster method is used (e.g., Le, 2020). There, single amorphous molecules are built by a random walk procedure with Monte Carlo methods. These molecules are put together in a simulation box with very low density (in the order of one third of the real system) and then equilibrated in a multi-stage process. Nevertheless, the method used here has some advantages. It is less complex, and due to the use of densely packed systems from the beginning, the proper use of barostats is possible. In addition, the method guarantees the real mixing and entanglement of the different chains, what is more difficult to achieve starting from coiled chains.

Starting from the proper melted state, the systems were cooled, again using a simulated annealing procedure under anisotropic pressure coupling. Different temperature profiles and cooling rates were tested to get models with different crystalline fractions and reduce simulation time. The exact procedures are discussed together with the obtained results in section 3.



$$OP_{ij} = \cos\left(\frac{\vec{r}_i \cdot \vec{r}_j}{|\vec{r}_i| \cdot |\vec{r}_j|}\right)$$

$$AOP(i) = \frac{1}{N} \cdot \sum_{j=1}^N OP_{ij}$$

Fig. 3. Principles of the order parameter used to distinguish crystalline from amorphous atoms

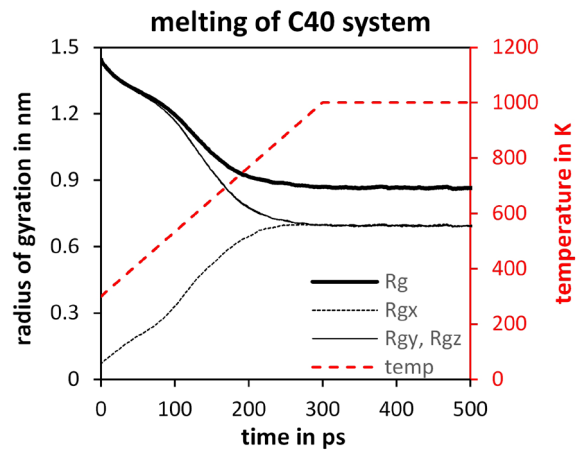
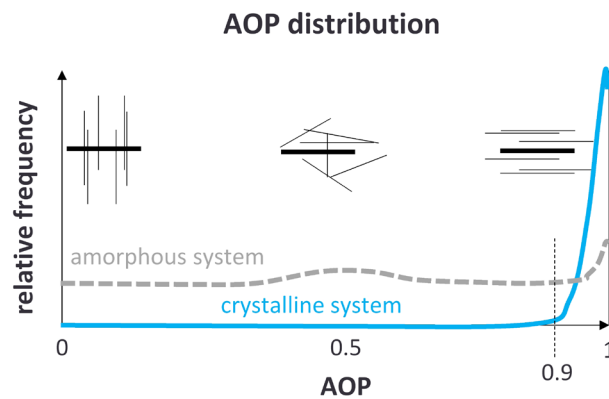


Fig. 2. Evaluation of the radius of gyration, R_g , with time during melting of the crystalline C40 system (chains initially aligned in the x -direction)

To distinguish atoms in crystalline state from those in an amorphous state, an order parameter was used (Fig. 3). For every carbon atom i in the simulation box the orientation of the chain vector r_i between the atoms $i - 2$ and $i + 2$ in the same chain was calculated. For crystalline phases, this vector should be parallel to the corresponding chain vectors of the surrounding atoms. As order parameter, called AOP in the following, the cosine of vector r_i and a surrounding vector r_j averaged over all nearest neighbour atoms within a distance of 0.65 nm from the central atom i , was calculated. From the distribution of the AOP value for all atoms in a crystalline system, a cut-off limit for AOP of 0.9 was set. In semi-crystalline systems every united atom i with $AOP > 0.9$ was classified as crystalline and crystallinity, c , was taken as the proportion of crystalline united atoms in the overall system. This procedure is not identical but very similar to procedures used by others (Lee & Rutledge, 2011).



2.4. Nanoindentation tests

From the different periodic bulk simulation boxes, surface boxes were obtained by stacking enough boxes together to form a model with at least 50 nm length in every direction. In order to form a surface and still be able to use the faster computational routines for 3D periodic systems, a vacuum slice of 150 nm was introduced by enlarging the simulation box in z -direction without changing atomic positions. The vacuum slice is large enough to avoid interactions between the periodic PE slices, so that periodicity in z -direction does not affect the surface. The simulation boxes were equilibrated to allow recombination at the freshly cleaved surface. The time which was necessary for equilibration varied again with chain length between 100 ps and 3 ns. The obtained surfaces were nearly flat for the amorphous and crystalline systems but showed distinct roughness for the semi-crystalline systems formed by the crystallites, which remained crystalline during the recombination process.

Since typical nanoindentation tests with Berkovich or Vickers indenter suffer from distinct size effects (Han et al., 2016) non-deformable indenters with a spherical tip were used in this work. A conical indenter with an opening angle of 25° was taken as the basic shape, and the tip was rounded with different radii of curvature. Regularly spaced positions on the outer surface of the tip were calculated mathematically and filled with atoms. These atoms had no interactions but fixed distances to each other to make the indenter non-deformable. Interactions between atoms of the indenter and the PE were chosen to be the same as between PE atoms.

The indenter was placed above the PE surface with at least 3 nm distance to the nearest surface atom (Fig. 4). The lowest atoms of the PE layer model were fixed in space to prevent movement of the entire model when external forces were applied. Starting from this state, two types of simulations were performed: distance controlled and force controlled indentation. For distance controlled indentation simulations the tip was moved a very small and defined distance towards the surface in z -direction at each time step by means of the “slow growth” mechanism in GROMACS. For the force controlled indentation tests, the indenter was moved towards the surface by a constant pulling force realized by the GROMACS “pull code”. In both cases, the indenter was the controlled element and could not be used for force assessment. Instead, the forces in z -direction were calculated from the sum of all forces in z -direction acting on the PE atoms.

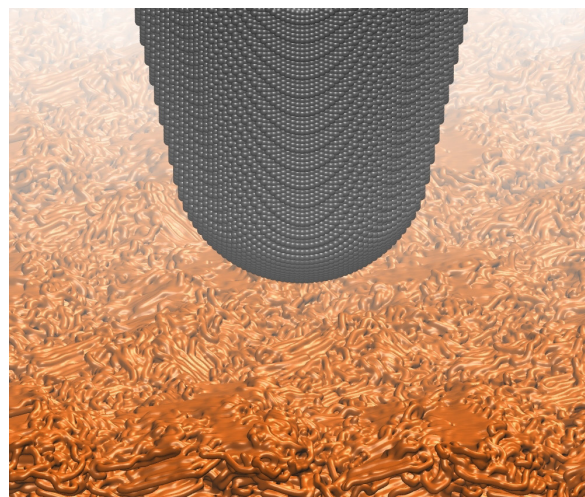


Fig. 4. Indentation tip with a radius of curvature of 8 nm above a semi-crystalline PE surface

3. Results and discussion

3.1. Semi-crystalline simulation boxes

In a first simulation run, the C160 melt was cooled from 600 K to 300 K within 900 ns, which means a cooling time of 3 ns/K or a cooling rate of 0.33 K/ns. The density of the system linearly increased with the decreasing temperature down to about 350 K. With further cooling a distinct deviation from linearity began (Fig. 5a) due to the formation and growth of small nuclei. The crystalline fraction increased and showed a linear relationship to the deviation of the density from linearity (Fig. 5b). At 300 K a crystalline fraction of 21% was reached, which remained stable during further simulations at a constant temperature.

As the simulation time was very long, an attempt was made to develop a more effective temperature program. Since crystallization only began below 350 K, the first cooling step was accelerated. The most effective procedure turned out to be rapid cooling to 350 K within 1 ns and subsequent slow cooling to 300 K with 3 ns/K. The crystalline fraction obtained was similar at 16%, but the simulation time could be significantly reduced from 900 ns to 150 ns. From Figure 6a it can be seen that the density was lower for the fast simulation compared to the slow simulation at temperatures above 350 K since the system was lagging behind equilibrium due to the high cooling rate. But, with slowing down the cooling the system reached a similar state as during the slow simulation and developed in an equal way. Deviations of the final density and the crystalline fraction were within typical ranges of multiple simulations.

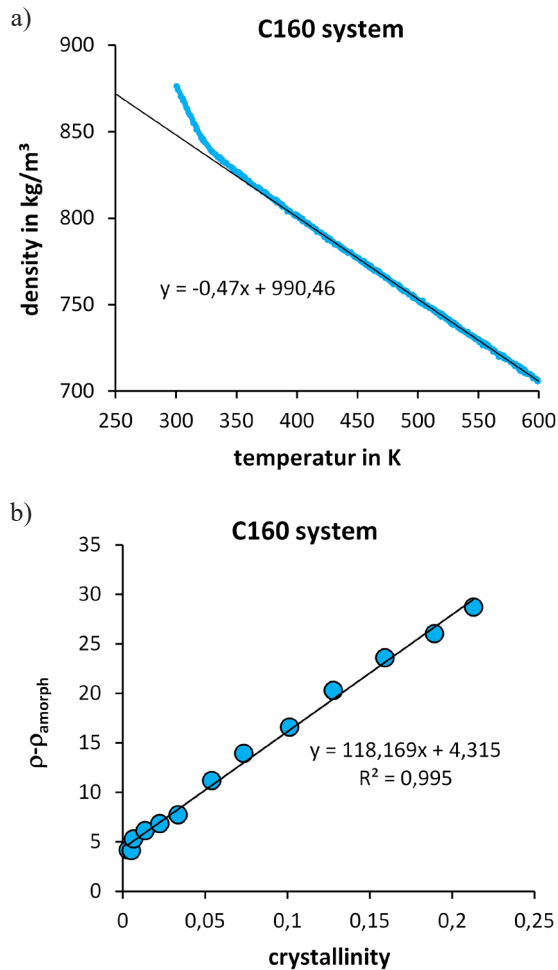


Fig. 5. Crystallization process of a C160 system: a) development of the density during cooling of the melt; b) deviation of the density from amorphous one depending on the current crystalline fraction

The final crystallinity depended on the chain length and the cooling rate (Fig. 6). For all simulations, fast cooling down to 350 K was used, and only the cooling rate in the lower temperature range was varied. For a system with a given chain length crystalline fraction increased approximately linear with increasing cooling time but then reached a plateau, which was higher for shorter chains. For C2000 chains, 50% seems to be a maximum value for crystallinity. Not even the introduction of additional isothermal phases at the crystallization temperature could further increase the crystalline fraction. But this value is often achieved as maximum crystallinity with homogeneous nucleation for PE, regardless of whether individual chains or whole melts were considered (Gao et al., 2016; Hu et al., 2018; Moyassari et al., 2019a). Higher crystalline fractions are only obtained by the use of external forces, which also leads to a preferred chain orientation.

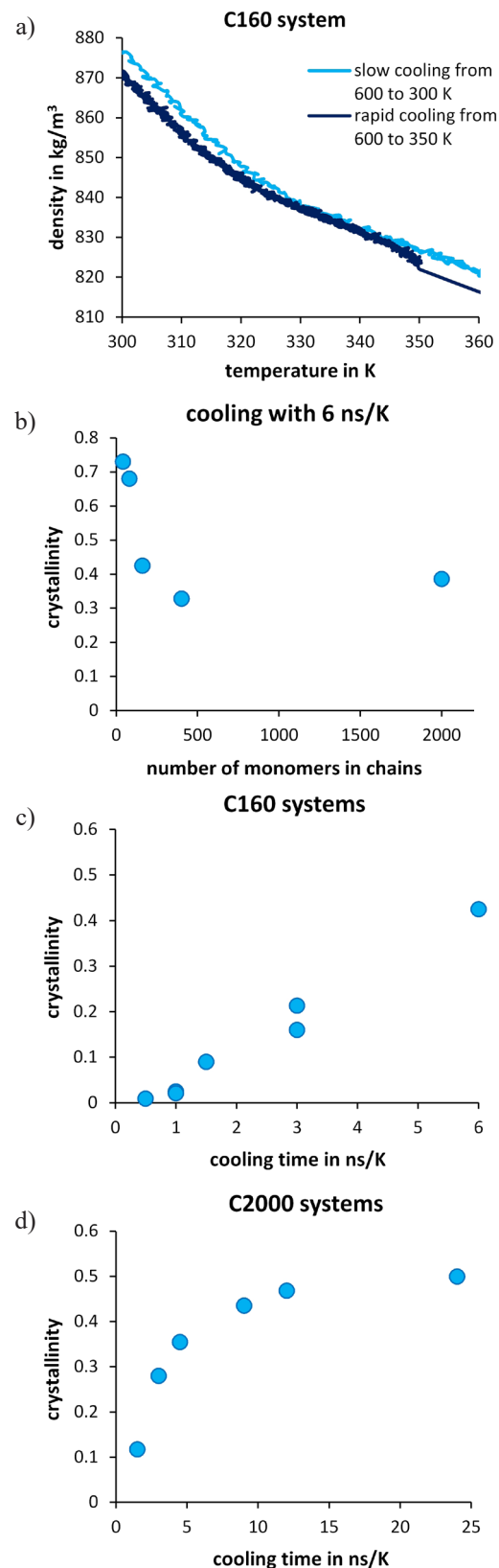


Fig. 6. Rate dependence of crystallization: a) development of the density for rapid cooling down to 350 K compared to the slow cooling from figure 4a; b) chain length dependence of the obtained crystalline fraction using the same cooling rate; c), d) cooling rate dependence of the crystalline fraction for the C160 and the C2000 system, respectively

The crystallization process in the form of successive snapshots of the simulation box is shown in Figure 7. Crystalline CH_2 -groups are coloured blue and amorphous ones grey. For a better representation of the spatial distribution perspective views of the final simulation boxes obtained with different cooling rates can be found in Figure 8. The crystallites vary in size and orientation, and the simulation boxes appear isotropic.

In Figure 9 selected single chains from the semi-crystalline simulation boxes with different chain length are shown, each one coloured differently for dif-

ferentiation. Within the C40 system, the crystallites are formed by fully stretched and perfectly aligned chains, whose head groups determine the boundaries of the crystallites. Between the crystallites there are single disordered chains, forming the amorphous interlayer. Almost no ties, loops, or partly crystalline molecules can be found. The C80 system already contains a few chains that are back folded or belong to two neighbouring crystallites. Systems with even longer chains form many kinks and ties, and chains are usually involved in several crystallites and amorphous interlayers.

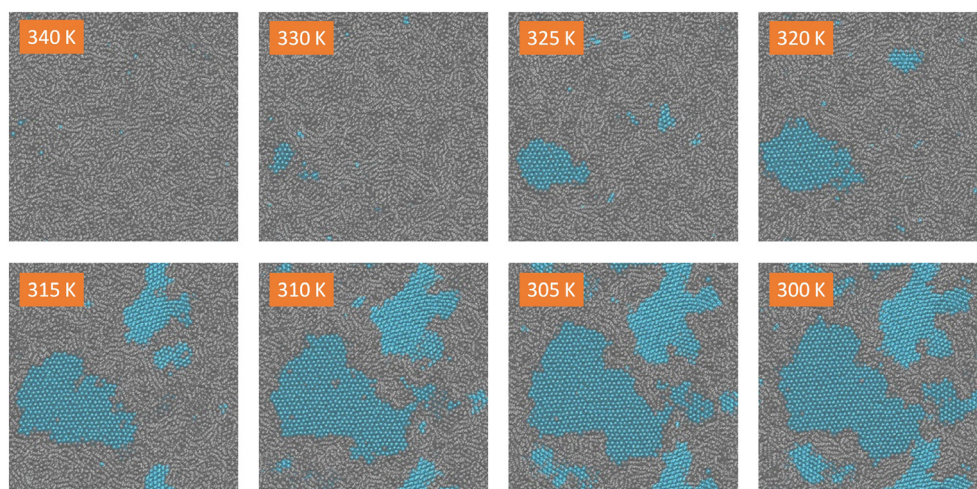


Fig. 7. Cross-section snapshots from the crystallization process of the C2000 system at different temperatures showing the nucleation and growth of crystallites (blue)

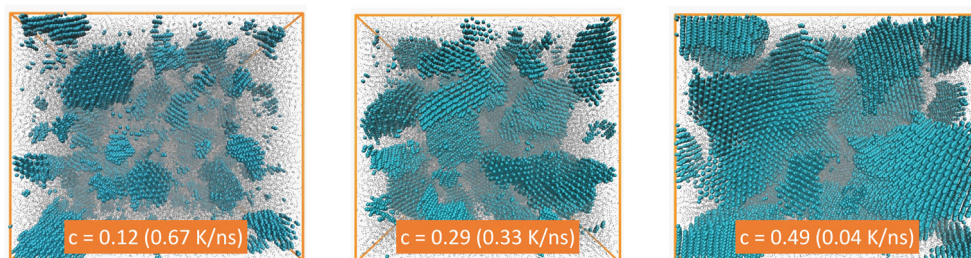


Fig. 8. Semi-crystalline simulation boxes with different crystallinity c and cooling rates in parenthesis; perspective view, simulation boxes are outlined in orange, crystalline monomers are shown as blue van der Waals-spheres, amorphous monomers as grey dots for better visibility of spatial distribution

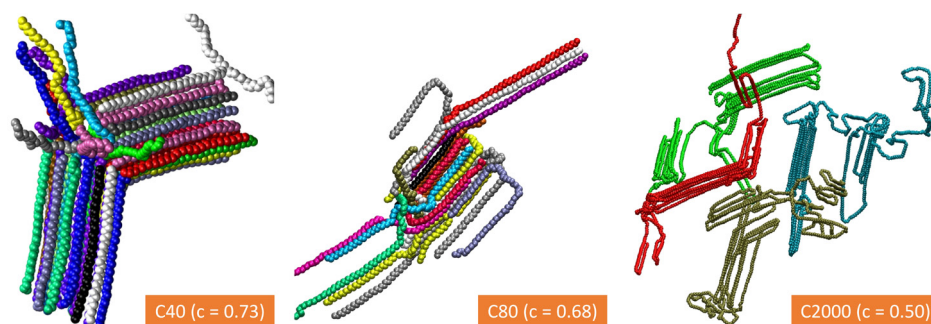


Fig. 9. Selected single chains from semi-crystalline simulation boxes with different chain lengths. Each chain is coloured differently for better differentiation

Even though the cooling rates used were very small and challenging for MD simulations, they were still orders of magnitude higher than during industrial crystallization processes. This is the reason why crystallites of industrial PE are much larger, which is accompanied by a more ordered structure and the formation of a dendritic superstructure. The cooling rate dependency is less pronounced, and crystallinity is almost exclusively determined by the branching of the molecules. Nevertheless, the simulated structures already show essential features of real semi-crystalline morphologies and are therefore better suited to study the influence of semi-crystallinity on mechanical properties and behaviour than the layered systems typically used to analyse the amorphous interphase (e.g., Kumar et al., 2017; Yeh et al., 2017). Using high cooling rates allows the creation of simulation boxes with different crystallinity from the same type of molecule, which is not quite simple in experiments. In this way, simulations can be used to distinguish between effects that originate from the crystallinity of the system and those that are caused by branching or chain length distribution. Adjusting the cooling rate allows targeted creation of simulation boxes, where the crystallinity can be controlled to an accuracy of a few percent.

The automated identification of crystallites from simulation snapshots or trajectories is quite challenging. Lee and Rutledge (2011) reviewed some methods to distinguish crystalline from amorphous atoms, but these are computationally expensive similar to the method used in this work. For a fast and easy way to determine the crystallinity of the system relationships between some physico-chemical system properties and the crystallinity can be exploited.

The most commonly used relation concerns the density of the system. Experimental data reveal a linear correlation between crystallinity and density. This could also be shown for simulations (Fig. 10a). If the chain length dependency (Fig. 10b) is also taken into account using the Fox–Flory equation (Fox & Flory, 1954), the density ρ of any system of linear chains with chain length N and crystallinity c can be calculated and vice versa:

$$\rho = \left[\rho_{\infty}^0 - \frac{k^0}{N} \right] \cdot (1 - c) + \left[\rho_{\infty}^1 - \frac{k^1}{N} \right] \cdot c \quad (1)$$

Here, ρ_{∞}^0 and k are the fitting parameters of the Fox–Flory equation for the amorphous system (superscript 0) and the crystalline system (superscript 1), respectively. The values for the GROMOS force field and a temperature of 300 K were obtained by the fit procedure in Figure 10b as follows: $\rho_{\infty}^0 = 859.6 \text{ kg/m}^3$, $k^0 = 1236.3$, $\rho_{\infty}^1 = 980.8 \text{ kg/m}^3$ and $k^1 = 1799.4$. Using this equation,

the deviation between calculated and simulated density was less than 0.5% for all obtained semi-crystalline simulation boxes. Conversely, the crystallinity of any system can now be estimated to about 2% accuracy based on the easily determined density.

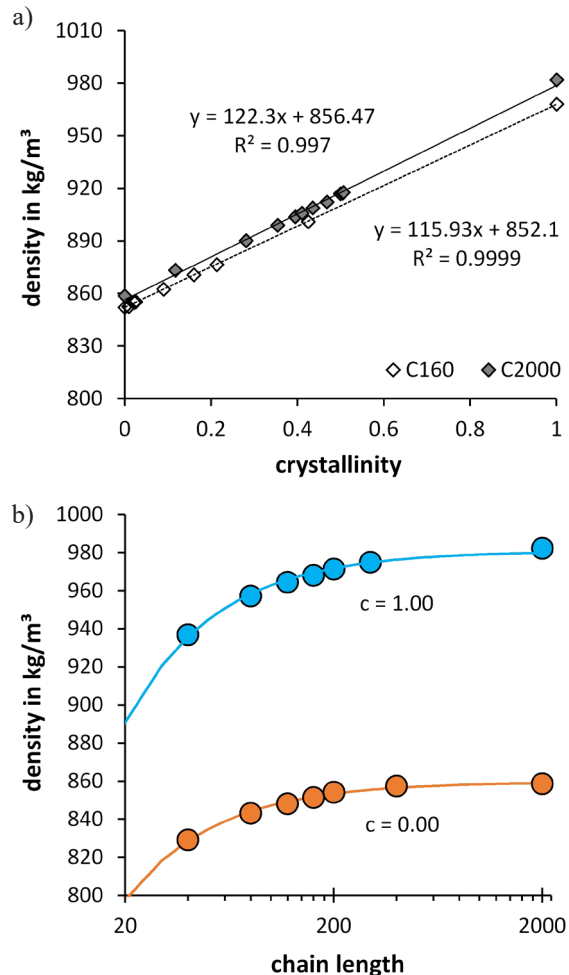


Fig. 10. Density of the systems depending on: a) the crystalline fraction; b) the chain length

A second fast and easy way to determine the crystallinity of a simulated system is the use of torsional angle distribution. A dihedral of 180° corresponds to the trans conformation, 0° to the cis conformation and 60° to the gauche conformation. A fully stretched chain is in all-trans state, coiled chains contain a certain degree of gauche angles to allow folding. Half of the symmetrical distribution is shown for different crystallinities of the C2000 system in Figure 11a. The heights of the trans and gauche peaks as well as their ratio show a distinct correlation with the crystallinity. However, the best correlation is obtained for the trans fraction, determined by integrating the normalized distribution for absolute angle values above 120° . This parameter has the great advantage to be chain length independent, as is shown in Figure 11b.

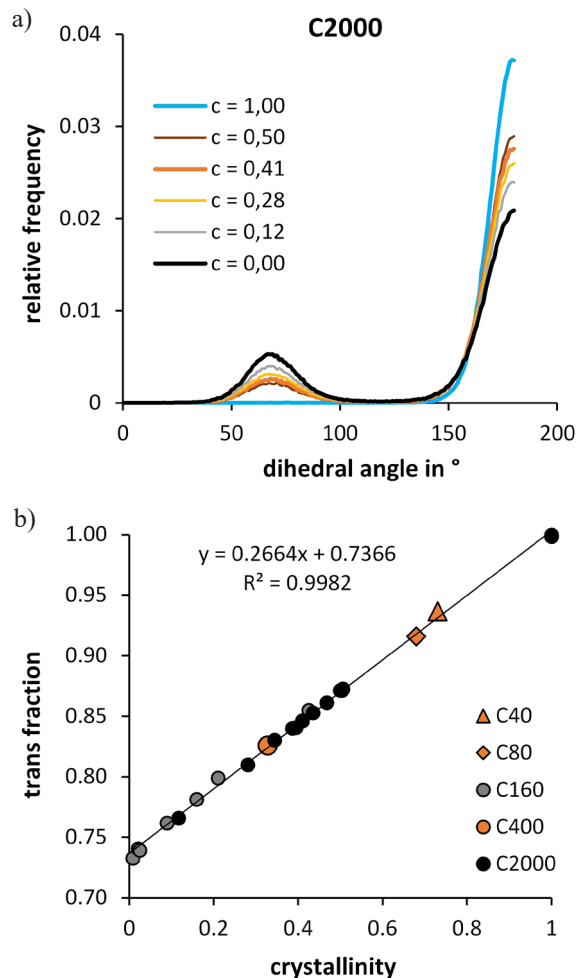


Fig. 11. Variation of dihedral angle distribution with crystallinity (a), and usage of trans fraction for determination of the crystalline fraction (b)

As a third possibility, different energy terms can be used to determine crystallinity, from which the

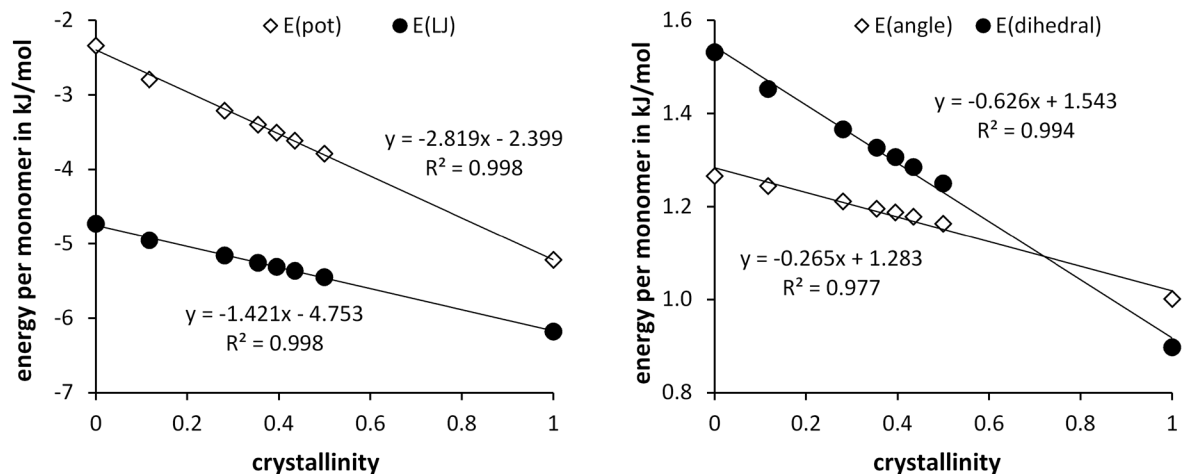


Fig. 12. Linear dependency between crystallinity and the per monomer values of potential, Lennard–Jones, bond, and dihedral energy terms for the example of the C2000 system

Lennard–Jones energy is the most suitable and pronounced one (Fig. 12). As per monomer values, the energy terms are independent of the chain length, as in the case of the trans fraction.

3.2. Nanoindentation tests

With the different semi-crystalline simulation boxes, nanoindentation tests were carried out with varying values for indenter tip radius, normal force, and velocity.

Some exemplary results from the force-controlled indentation tests are shown in Figure 13a. For the crystalline system, the applied normal force of 5 nN only caused elastic deformation. Initially, there are some vibrations in the penetration depth curve originating from the settling of the indenter in connection with the force control, but then the penetration depth remains constant as expected for a crystalline system like a metal. For the amorphous system the settling vibrations are nearly completely damped, and the penetration depth increases with increasing simulation time. The behaviour of the semi-crystalline system lies in between, showing medium hardness, damping and resistance. But, while the indentation curves for different crystallinities differ strongly, the force-relaxation curves show similar characteristics (Fig. 13b). Here, the indenter was penetrated about 8 nm deep into the material by distance controlled simulations. Then, the indenter was held at a constant position while the PE was allowed to relax, and the normal force was monitored. As expected, starting and final forces increase with increasing crystallinity yet the relaxation velocity and amount are nearly the same for all considered systems.

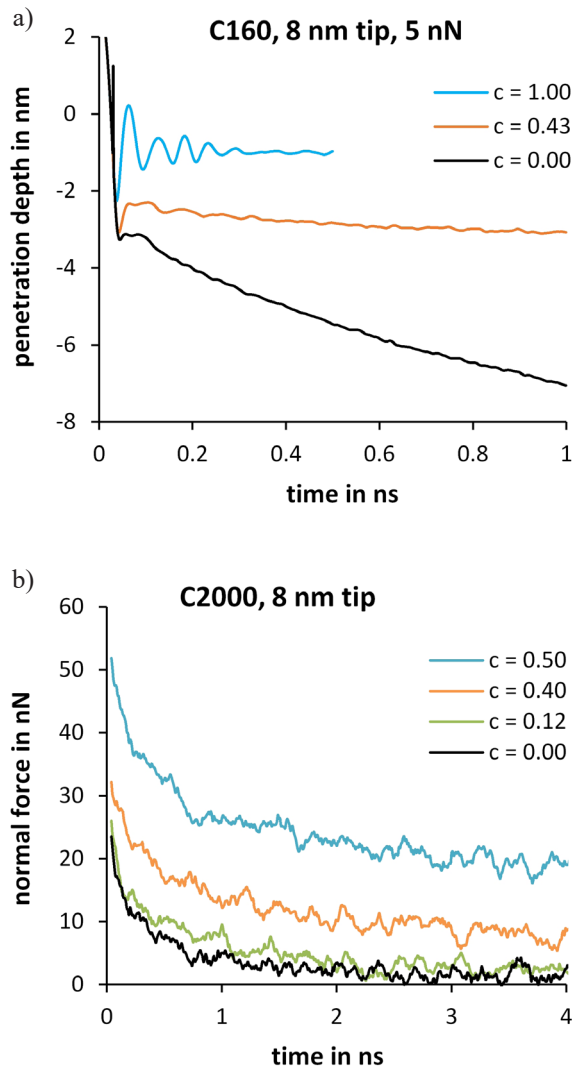


Fig. 13. Effect of crystallinity on force-controlled indentation tests (a), and force relaxation (b)

The determined normal forces during distance-controlled nanoindentation tests with C160 systems of different crystallinity are shown in Figure 14. In each case the tip was penetrated about 10 nm deep into the surface with a velocity of 20 m/s and then retracted. The force within the indentation part of the simulation increased in slope with increasing crystallinity as expected. For crystalline and semi-crystalline systems, deviations from linearity mark the region of plastic deformation of the crystals. During the retraction of the indenter there were distinct negative adhesion forces due to the interactions between indenter and substrate. While the work of adhesion was similar for all cases, the distribution of adhesion forces was strongly dependent on crystallinity. At high crystallinity, the PE chains are more tightly bound to the substrate, causing a comparatively sharp tear-off. In contrast, the amorphous PE chains move more easily. The maximum adhesion force is much smaller and chains cling to the indenter tip much longer. Cross-section snapshots of the simulations with colour-coded deformation of the PE are shown in Figure 15.

As can be seen from the pictures of the amorphous system in Figure 15, the surface of PE is depressed with the indentation. The penetration depth of the indenter lacks behind the travelled distance relative to the initial surface position. The volume affected by nanoindentation is symmetrical and enlarges with penetration depth. Atoms are not displaced if they are more than approximately three times of the penetration depth away from the tip. The deformation is plastic in the sense of a real displacement of the chains against each other. But, with the retraction of the indenter adhered material is lifted by adhesion, and almost no imprint remains.

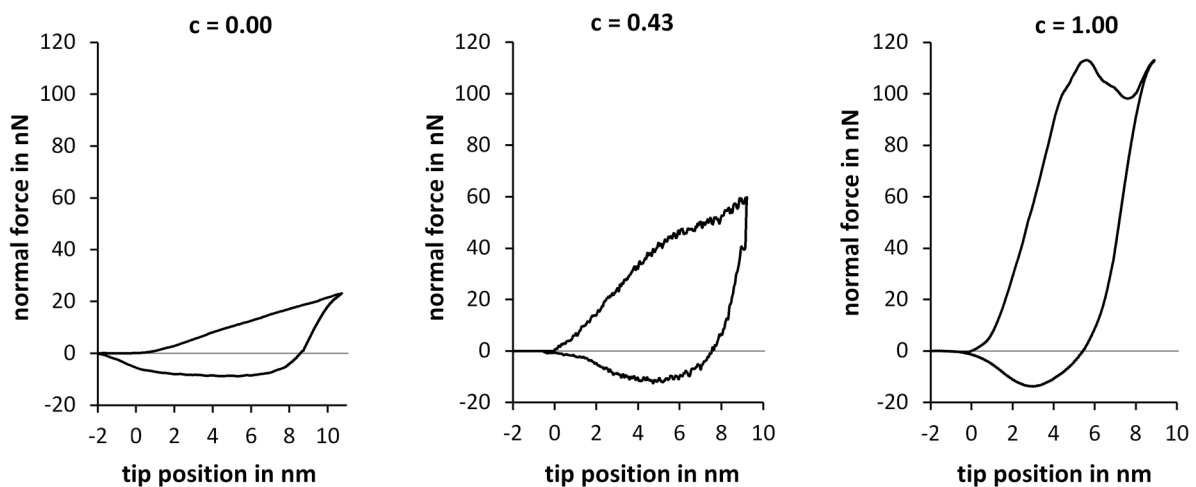


Fig. 14. Nanoindentation curves for C160 systems with different crystallinity c ; a tip position of 0 corresponds to the initial position of the surface

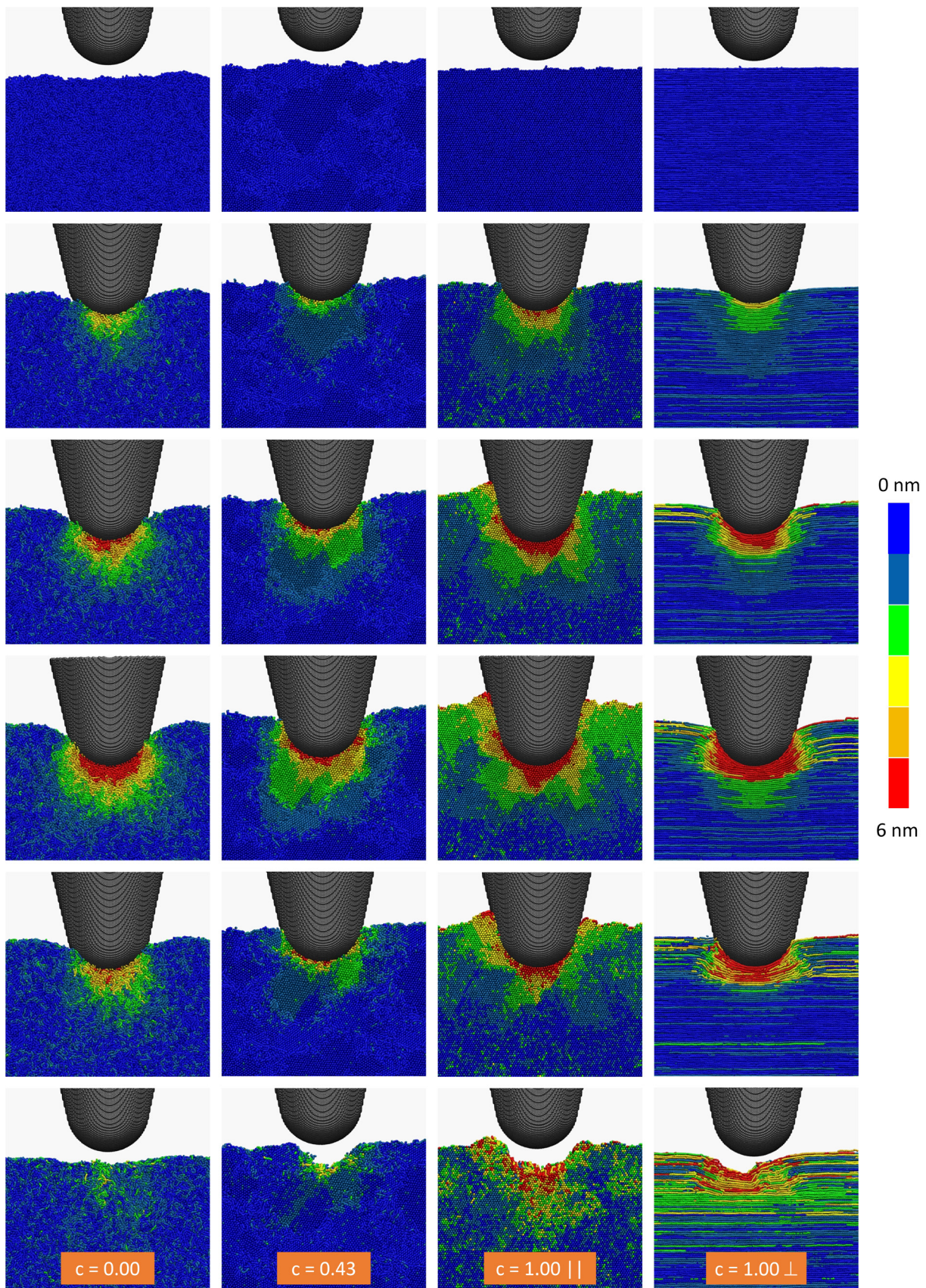


Fig. 15. Cross-section snapshots of the simulation boxes from the nanoindentation tests of figure 14 with colour-coded deformation of the PE compared to the initial state. The viewing direction for the crystalline model is parallel (3rd column) and perpendicular (4th column) to the chain direction

For small penetration depths up to 5 nm the crystalline system only exhibits elastic behaviour. Chains are bent down and slightly compressed but not moved against each other. Beyond 5 nm of penetration depth, dislocations occur and whole parts of the crystal are shifted against each other. By retraction of the indenter, a distinct imprint remains with amorphous chains at the surface. In the bottom pictures of Figure 15 the deformation of the green coloured chains is caused by lateral movement in chain direction, what is not prevented within an artificial system of fully aligned chains.

Deformation of the semi-crystalline system is strongly determined by the positions of the crystallites (Fig. 15). Crystallites beneath the indenter tip are shifted as a whole within the amorphous matrix. There may be some deformation of the crystallites shape, but the chains keep their crystalline alignment. The shifting direction depends on the position of other crystallites and the direction of the acting forces. The region that is affected by the indentation becomes strongly inhomogeneous. Due to the strong cross-linking of the single

crystallites by tie molecules, the structure recovers well during retraction and only the uppermost chains deform plastically, leaving a clear remaining imprint.

When the tip approaches the surface, there are some measurable interactions attracting the tip to the surface, the so-called “snap-in” (Fig. 16a). With further approach, direct contact arises, the material has to be removed, and the forces become repulsive. This point was taken as the initial surface position. In the case of rough, semi-crystalline surfaces, especially for indenters with large tip radius, the contact between tip and surface is not uniform for small penetration depths, which leads to a non-linear increase of the force. For large penetration depths, plastic deformation may occur, but in between the force-displacement-curves exhibit linear regions. The slope of this region is referred to as contact stiffness in the following. This contact stiffness is strongly dependent on crystallinity, tip radius, and velocity (Figs. 16b and 17). No chain length dependency could be found except for very short chains (C40, C80) that exhibit distinctly lower contact stiffness due to the lack of tie molecules (compare Fig. 9).

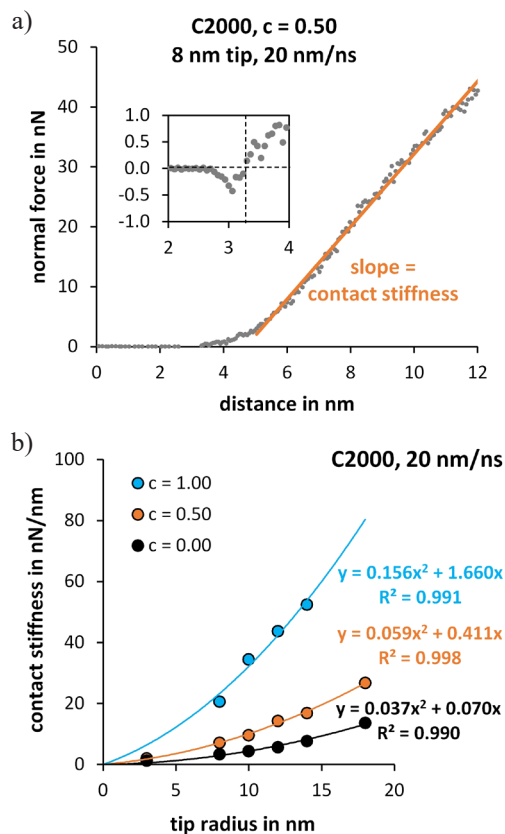


Fig. 16. Definition of contact stiffness as slope of the linear part of the indentation curve (a) – the inset shows the “snap-in” region of the first contact between surface and tip used for determination of initial surface position; dependency of contact stiffness on tip radius for various crystallinities (b)

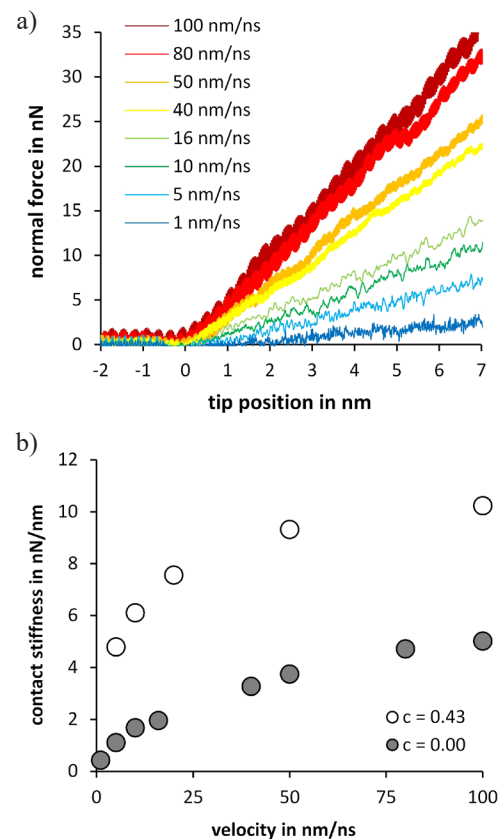


Fig. 17. Force-displacement-curves from indentation tests with different velocities for the amorphous C160 system (a), and velocity dependency of the contact stiffness for the amorphous and a semi-crystalline C160 system (b); for comparison: the contact stiffness of the crystalline C160 system (not shown) has constant values of around 25 nN/nm

4. Conclusions

In this paper it was shown how semi-crystalline simulation boxes of polyethylene, suited for the investigation of mechanical properties by MD simulations can be created in a targeted manner by nucleation from the melt. Extensive melting prior to the crystallization guarantees good mixing, inter chain contact and entanglement of the PE chains in the melt. In turn, this leads to high cross-linking of the formed crystallites since every PE chain is involved in several crystallites. The chain length and cooling rate are the main parameters that affect the obtained crystalline fraction using non-isothermal crystallization simulations of linear PE chains. Various parameters were presented by which the crystallinity of the system can be estimated both rapidly and easily. The semi-crystalline simulation boxes contain a multitude of crystallites of randomly distributed sizes and orientations. The boxes are nearly isotropic and reflect the main features of a semi-crystalline polymeric structure.

The semi-crystalline simulation boxes were transformed into semi-crystalline surface models and subjected to nanoindentation tests. The mechanical response of the simulated PE was determined by the crystallinity as it is expected from experiments. The simulations further reveal the time and rate dependen-

cy typical for viscoelastic materials. The usage of such semi-crystalline simulation boxes now permits insight to be gained into materials behaviour that cannot be obtained by analysing purely amorphous or purely crystalline systems. Besides the understanding of nanoindentation and polymeric deformation behaviour, the results are also important for contact mechanics.

Acknowledgement

The presented results are part of two research projects (“Experiments and simulations regarding micro friction”, VF160047, and “Estimation of the real contact area”, 49VF190053). Both projects were partly funded by the German Federal Ministry for Economic Affairs and Energy (BMWi) based on a resolution of the German Bundestag via the project management organization EuroNorm GmbH. Our thanks are extended for the support granted.

Gefördert durch:



aufgrund eines Beschlusses
des Deutschen Bundestages

References

- Abraham, M.J., Murtola, T., Schulz, R., Páll, S., Smith, J.C., Hess, B., & Lindahl, E. (2015). GROMACS: High performance molecular simulations through multi-level parallelism from laptops to supercomputers. *SoftwareX*, 1–2, 19–25.
- Abu-Sharkh, B., & Hussein, I.A. (2002). MD simulation of the influence of branch content on collapse and conformation of LLDPE chains crystallizing from highly dilute solutions. *Polymer*, 43(23), 6333–6340.
- Allen, M.P., & Tildesley, D.J. (1987). *Computer Simulation of Liquids*. Clarendon Press.
- Anwar, M., & Schilling, T. (2015). Crystallization of polyethylene: A molecular dynamics simulation study of the nucleation and growth mechanisms. *Polymer*, 76, 307–312.
- Berendsen, H.J.C., Postma, J.P.M., Gunsteren, W.F. van, DiNola, A., & Haak, J.R. (1984). Molecular dynamics with coupling to an external bath. *The Journal of Chemical Physics*, 81(8), 3684–3690.
- Berendsen, H.J.C., Spoel, D. van der, & Drunen van, R. (1995). GROMACS: A message-passing parallel molecular dynamics implementation. *Computer Physics Communications*, 91(1–3), 43–56.
- Bussi, G., Donadio, D., & Parrinello, M. (2007). Canonical sampling through velocity rescaling. *The Journal of Chemical Physics*, 126(1), 014101.
- Christöfl, P., Czibula, C., Berer, M., Oreski, G., Teichert, C., & Pinter, G. (2021). Comprehensive investigation of the viscoelastic properties of PMMA by nanoindentation. *Polymer Testing*, 93, 106978.
- Daura, X., Mark, A.E., & Gunsteren, W.F.J. van (1998). Parametrization of Aliphatic CH_n United Atoms of GROMOS96 Force Field. *Journal of Computational Chemistry*, 19(5), 535–547.
- Doran, M., & Choi, P. (2001). Molecular dynamics studies of the effects of branching characteristics on the crystalline structure of polyethylene. *The Journal of Chemical Physics*, 115(6), 2827–2830.
- Fox, T.G., & Flory, P.J. (1954). The glass temperature and related properties of polystyrene. Influence of molecular weight. *Journal of Polymer Science*, 14(75), 315–319.
- Frenkel, D., & Smit, B. (2001). *Understanding molecular simulation: from algorithms to applications* (2nd ed.). Academic Press.
- Gao, R., He, X., Shao, Y., Hu, Y., Zhang, H., Liu, Z., & Liu, B. (2016). Effects of Branch Content and Branch Length on Polyethylene Crystallization: Molecular Dynamics Simulation. *Macromolecular Theory and Simulation*, 25(3), 303–311.
- Gibson, R.F. (2014). A review of recent research on nanoindentation of polymer composites and their constituents. *Composites Science and Technology*, 105, 51–65.

- Gromacs. Fast. Flexible. Free* (2020), <https://www.gromacs.org/>.
- Hall, K.W., Sirk, T.W., Percec, S., Klein, M.L., & Shinoda, W. (2020). Monodisperse Polymer Melts Crystallize via Structurally Polydisperse Nanoscale Clusters: Insights from Polyethylene. *Polymers*, *12*(2), 447.
- Han, C.-S., Saneii, S.Y.R., & Alisafaei, F. (2016). On the origin of indentation size effects and depth dependent mechanical properties of elastic polymers. *Journal of Polymer Engineering*, *36*(1), 103–111.
- Higuchi, Y. (2019). Stress Transmitters at the Molecular Level in the Deformation and Fracture Processes of the Lamellar Structure of Polyethylene via Coarse-Grained Molecular Dynamics Simulations. *Macromolecules*, *52*(16), 6201–6212.
- Higuchi, Y., & Kubo, M. (2017). Deformation and Fracture Processes of a Lamellar Structure in Polyethylene at the Molecular Level by a Coarse-Grained Molecular Dynamics Simulation. *Macromolecules*, *50*(9), 3690–3702.
- Hill, T.L. (1987). *An Introduction to Statistical Thermodynamics*. Dover Publications.
- Hockney, R.W., Goel, S.P., & Eastwood, J. (1974). Quiet High Resolution Computer Models of a Plasma. *Journal of Computational Physics*, *14*(2), 148–158.
- Hollingsworth, S.A., & Dror, R.O. (2018). Molecular Dynamics Simulation for All. *Neuron*, *99*(6), 1129–1143.
- Hossain, D., Tschopp, M.A., Ward, D.K., Bouvard, J.L., Wang, P., & Hostemeyer, M.F. (2010). Molecular dynamics simulations of deformation mechanisms of amorphous polyethylene. *Polymer*, *51*(25), 6071–6083.
- Hu, E., Sun, Y., Zeng, F., & Qu, J. (2011). Nanoindentation simulation of PE/POSS under different shapes of indenters. *Acta Mechanica Solida Sinica*, *24*(4), 365–372.
- Hu, E., Sun, Y., & Zeng, F. (2013). The enhancement mechanism and deformation analysis of polyethylene incorporated with POSS by nanoindentation simulation. *Reviews on Advanced Materials Science*, *33*(1), 85–91.
- Hu, Y., Shao, Y., Liu, Z., He, X., & Liu, B. (2018). Effect of short-chain branching on the tie chains and dynamics of bimodal polyethylene: Molecular dynamics simulation. *European Polymer Journal*, *103*, 312–321.
- Jabbari-Farouji, S., Rottler, J., Lame, O., Makke, A., Perez, M., & Barrat, J.-L. (2015). Plastic Deformation Mechanisms of Semi-crystalline and Amorphous Polymers. *ACS Macro Letters*, *4*(2), 147–150.
- Kim, J.M., Locker, R., & Rutledge, G.C. (2014). Plastic Deformation of Semi-crystalline Polyethylene under Extension, Compression, and Shear Using Molecular Dynamics Simulation. *Macromolecules*, *47*(7), 2515–2528.
- Ko, M.J., Waheed, N., Lavine, M.S., & Rutledge, G.C. (2004). Characterization of polyethylene crystallization from an oriented melt by molecular dynamics simulation. *The Journal of Chemical Physics*, *121*(6), 2823.
- Kumar, V., Locker, C.R., Veld, P.J. in't, & Rutledge, G.C. (2017). Effect of Short Chain Branching on the Interlamellar Structure of Semi-crystalline Polyethylene. *Macromolecules*, *50*(3), 1206–1214.
- Lacevic, N., Fried, L.E., & Gee, R.H. (2008). Heterogeneous directional mobility in the early stages of polymer crystallization. *The Journal of Chemical Physics*, *128*(1), 014903.
- Lavine, M.S., Waheed, N., & Rutledge, G.C. (2003). Molecular dynamics simulation of orientation and crystallization of polyethylene during uniaxial extension. *Polymer*, *44*(5), 1771–1779.
- Lazim, R., Suh, D., & Choi, S. (2020). Advances in Molecular Dynamics Simulations and Enhanced Sampling Methods for the Study of Protein Systems. *International Journal of Molecular Sciences*, *21*(17), 6339.
- Le, T.-T. (2020). Analysis of elastic deformation of amorphous polyethylene in uniaxial tensile test by using molecular dynamics simulation. *Computer Methods in Materials Science*, *20*(2), 38–44.
- Lee, S., & Rutledge, G.C. (2011). Plastic Deformation of Semicrystalline Polyethylene by Molecular Simulation. *Macromolecules*, *44*(8), 3096–3108.
- Liao, Q., & Jin, Y. (1999). Formation of segmental clusters during relaxation of a fully extended polyethylene chain at 300 K: A molecular dynamics simulation. *The Journal of Chemical Physics*, *110*(17), 8835.
- Lindahl, E., Abraham, M.J., Hess, B., & van der Spoel, D. (2021a). *GROMACS 2021 Manual (Version 2021)*. Zenodo. <http://doi.org/10.5281/zenodo.4457591>.
- Lindahl, E., Abraham, M.J., Hess, B., & van der Spoel, D. (2021b). *GROMACS 2021 Source code (Version 2021)*. Zenodo. <http://doi.org/10.5281/zenodo.4457626>.
- Meguid, S.A., Alian, A.R., & Dewapriya, M.A.N. (2018). Atomistic Modelling of Nanoindentation of Multilayered Graphene-Reinforced Nanocomposites. In S. Meguid, G. Weng (Eds.), *Micromechanics and Nanomechanics of Composite Solids* (pp. 39–70). Springer.
- Monasse, B., Queyroy, S., & Lhost, O. (2008). Molecular Dynamics prediction of elastic and plastic deformation of semi-crystalline polyethylene. *International Journal of Material Forming*, *1* (supplement issue 1), 1111–1114.
- Moyassari, A., Gkourmpis, T., Hedenqvist, M.S., & Gedde, U.W. (2019a). Molecular Dynamics Simulations of Short-Chain Branched Bimodal Polyethylene: Topological Characteristics and Mechanical Behavior. *Macromolecules*, *52*(3), 807–818.
- Moyassari, A., Gkourmpis, T., Hedenqvist, M.S., & Gedde, U.W. (2019b). Molecular dynamics simulation of linear polyethylene blends: Effect of molar mass bimodality on topological characteristics and mechanical behavior. *Polymer*, *161*, 139–150.
- Oostenbrink, C., Villa, A., Mark, A.E., & Gunsteren, van W.F. (2004). A Biomolecular Force Field Based on the Free Enthalpy of Hydration and Solvation: The GROMOS Force-Field Parameter Sets 53A5 and 53A6. *Journal of Computational Chemistry*, *25*(13), 1656–1676.
- Páll, S., & Hess, B. (2013). A flexible algorithm for calculation pair interactions on SIMD architectures. *Computer Physics Communications*, *184*(12), 2641–2650.
- Peng, C., & Zeng, F. (2017). A molecular simulation study to the deformation behavior and the size effect of polyethylene during nanoindentation. *Computational Materials Science*, *137*, 225–232.
- Poly(ethene) (Polyethylene)* (2017). The Essential Chemical Industry – online, <https://www.essentialchemicalindustry.org/polymers/polyethene.html>.

- Ramos, J., & Martínez-Salazar, J. (2011). Computer Modeling of the Crystallization Process of Single-Chain Ethylene/1-Hexene Copolymers from Dilute Solutions. *Journal of Polymer Science Part B: Polymer Physics*, 49(6), 421–430.
- Ramos, J., Vega, J.F., & Martínez-Salazar, J. (2018). Predicting experimental results for polyethylene by computer simulation. *European Polymer Journal*, 99, 298–331.
- Rozanski, A., & Galeski, A. (2013). Plastic yielding of semi-crystalline polymers affected by amorphous phase. *International Journal of Plasticity*, 41, 14–29.
- Ruestes, C.J., Alhafez, I.A., & Urbassek, H.M. (2017). Atomistic Studies of Nanoindentation – A Review of Recent Advances. *Crystals*, 7(10), 293.
- Sanmartín, S., Ramos, J., & Martínez-Salazar, J. (2012). Following the Crystallization Process of Polyethylene Single Chain by Molecular Dynamics: The Role of Lateral Chain Defects. *Macromolecular Symposia*, 312(1), 97–107.
- Sanmartín, S., Ramos, J., Vega, J.F., & Martínez-Salazar, J. (2014). Strong influence of branching on the early stage of nucleation and crystal formation of fast cooled ultralong *n*-alkanes as revealed by computer simulation. *European Polymer Journal*, 50, 190–199.
- Schuler, L.D., Daura, X., & Gunsteren, W.F.J. van (2001). An Improved GROMOS96 Force Field for Aliphatic Hydrocarbons in the Condensed Phase. *Journal of Computational Chemistry*, 22(11), 1205–1218.
- VanLandingham, M.R., Villarrubia, J.S., Guthrie, W.F., & Meyers, G.F. (2001). Nanoindentation of Polymers: An Overview. *Macromolecular Symposia*, 167(1), 15–43.
- Verho, T., Paajanen, A., Vaari, J., & Laukkanen, A. (2018). Crystal Growth in Polyethylene by Molecular Dynamics: The Crystal Edge and Lamellar Thickness. *Macromolecules*, 51(13), 4865–4873.
- Voyiadjis, G.Z., & Yaghoobi, M. (2017). Review of Nanoindentation Size Effect: Experiments and Atomistic Simulation. *Crystals*, 7(10), 321.
- Wang, J., Zhao, L., Song, M., Hu, F., & He, X. (2021). Molecular dynamics simulation for polyethylene crystallization: the effect of long chain branches. *Polyolefins Journal*, 8(2), 73–84. <https://doi.org/10.22063/poj.2021.2834.1173>.
- Xu, M., Huang, G., Feng, S., McShane, G.J., & Stronge, W.J. (2016). Static and Dynamic Properties of Semi-Crystalline Polyethylene. *Polymers*, 8(4), 77.
- Yashiro, K., Furuta, A., & Tomita, Y. (2006). Nanoindentation on crystal/amorphous polyethylene: Molecular dynamics study. *Computational Materials Science*, 38(1), 136–143.
- Yeh, I.-C., Andzelm, J.W., & Rutledge, G.C. (2015). Mechanical and Structural Characterization of Semi-crystalline Polyethylene under Tensile Deformation by Molecular Dynamics Simulations. *Macromolecules*, 48(12), 4228–4239.
- Yeh, I.-C., Lenhart, J.L., Rutledge, G.C., & Andzelm, J.W. (2017). Molecular Dynamics Simulation of the Effects of Layer Thickness and Chain Tilt on Tensile Deformation Mechanisms of Semi-crystalline Polyethylene. *Macromolecules*, 50(4), 1700–1712.
- Zhang, J., Wang, Z., Yan, Y., & Sun, T. (2016). Concise Review: Recent Advances in Molecular Dynamics Simulation of Nanomachining of Metals. *Current Nanoscience*, 12(6), 653–665.